Hindawi
Journal of Spectroscopy
Volume 2021, Article ID 6629640, 12 pages
https://doi.org/10.1155/2021/6629640

Research Article

Spectroscopic Analysis for Harnessing the Quality and Potential of Gemstones for Small and Medium-Sized Enterprises (SMEs)

Imtiaz Ahmad,[1] **Suhail H. Serbaya**,[2] **Ali Rizwan**,[2] **and Malik Sajjad Mehmood**[1]

[1]*Department of Basic Sciences, University of Engineering and Technology, Taxila, Pakistan*
[2]*Department of Industrial Engineering, King Abdulaziz University, Jeddah 21589, Saudi Arabia*

Correspondence should be addressed to Malik Sajjad Mehmood; msajjad.82@gmail.com

Received 9 December 2020; Revised 4 April 2021; Accepted 28 June 2021; Published 9 July 2021

Academic Editor: Daniel Cozzolino

Introduction of modern technologies and methods and quality analysis for the gemstone industry are the main strategic initiatives of the Small and Medium Development Authority (SMEDA) of Pakistan. In this regard, four natural gemstones Quartz, Pyrope-Almandine Garnet, Black tourmaline, and Amethyst brought from Hunza valley Pakistan were analyzed by state-of-the-art spectroscopic techniques including EDX, UV-VIS, and FTIR spectroscopy. EDX revealed the traces of Fe, Mg, and Ca in Pyrope-Almandine garnet, Mg and Fe in Black tourmaline, Au and Ca in Amethyst. UV-VIS data revealed the values of Urbach energies 520, 210, 460, and 430 meV, and the values of direct bandgap energies 5.14, 6.12, 5.54, 5.74 eV, respectively. The higher structural disorder due to the presence of Fe and other impurities in stones except Quartz was attributed to the higher values of Urbach energies and decrease in band gaps: FTIR data Fe-O and Si-O stretching vibration in Pyrope-Almandine garnet, Si-O bending vibrations and O-H stretching vibration in Quartz, Si-O-Si bending and stretching vibrations and C=O stretching vibrations in Black tourmaline, Ca-O stretching vibrations and Si-OH weak-vibrations in Amethyst. Photoluminescence results also showed useful information in investigating the properties of gemstones.

1. Introduction

Mineral deposits play a vital role in the economic development of a country, and in this regard, Pakistan is well known for its abundance of natural resources and beauty. Especially northern and northwestern areas are rich with minerals incorporating precious and semiprecious gemstones. Of particular importance, these areas are blessed with huge reservoirs of ruby, sapphire, spinel, emerald, Quartz, topaz, tourmaline, and aquamarine. The aforementioned types/classes of gemstones have great significance due to their wide use in jewelry, as well as in electronic, instrument, and scientific tools. It is, therefore, necessary to identify and distinguish natural gemstones from their synthetic counterparts to avoid the imitation of natural ones. Most of the gemstones are colorless in nature and they are colored by some trace elements as impurities. These trace elements can serve as fingerprints for the identification and provenance of gemstones. Identification of gemstones has significant value for the commercial trade of natural gemstones. Therefore, a robust qualitative and quantitative analytical technique is required for distinguishing synthetic and natural gemstones. In this regard, refractometers, polariscopes, hand spectroscope, and microscopes were being used in gemstones identification in the past. Nowadays, most sophisticated techniques like ultraviolet visible (UV-VIS) spectrometer, Raman spectroscopy, infrared spectroscopy, electron dispersive X-ray spectroscopy, and X-ray fluorescence (XRF) are used for detail qualitative and quantitative analysis of natural gemstones in order to separate them from their artificial counterpart [1–4].

The color of the natural gemstones is the basic factor for determining the quality and commercial significance, and there are multiple factors for the origin of these colors in gem minerals [2, 5–7]. Geologists have identified the following five mechanisms which are responsible for the color of gemstones [8–10].

(i) Disperse metal ions causes the color in the gemstones. Illumination of dispersed metal ions by a light source absorbs certain wavelengths and can cause the electrons to jump to some temporary higher state. Luminescence is emitted as energy from electrons and confers color to the gemstones. The recognition of the ion is not the only factor that can affect the color of gemstones; other factors like the valence state, nature of neighboring atoms, and ion coordination also take part in coloration in gemstones.

(ii) When the absorption occurs, then electrons jump from one atom to another atom that causes the coloration of the gemstones.

(iii) Irradiation of gemstones can affect the metal ions and change their oxidation state along with the color center.

(iv) Absorption can be occurred due to the transition of energy bands that can cause the color.

(v) Phenomena like interference, scattering, diffraction, and inclusion can change the color of gemstones.

In order to have fully explored the nature of scientific phenomena responsible for giving color to gemstones, various spectroscopic methodologies including UV-VIS, FTIR, XRD, XRF, EDX spectroscopy, are used [11–13]. In this regard, Kassem et al. [14] have characterized the Quartz sample (milky color) belonging to a wadi of the eastern desert of Egypt, i.e., Araba, while using a number of techniques including SEM, XRD, UV-VIS, FTIR, XRF, and inductively coupled plasma-optical emission spectra (ICP-OES) and electron spin resonance (ESR) technique to assess the radiation treatment effect on the color of Quartz. The FTIR spectra results revealed the increased absorption bands for $[Al\text{- }OH/Na]^+$ and $[Al\text{-}OH/Li]^+$ on irradiation. UV-VIS spectra reveal an increase in bandgap properties on irradiation while ESR spectroscopy has shown a significant increase in peak intensity. Although Kassem et al. [14] have used many techniques, unfortunately, the correlation among the results of different experimental techniques is missing to have a solid conclusion. In another study, Branca et al. [15] utilized the SEM, XRD, Raman, and FTIR spectroscopy for a qualitative investigation of five types of emerald samples from different localities. They have used the Gaussian deconvolution for the identification/quantification of OH and Si-O contents while figuring out the hidden peaks in 3400–3800 cm^{-1} and 1000–1300 cm^{-1}, respectively. In addition to peak deconvolution, they also used spectral differentiation for establishing the proper correlation for alkali contents within the beryl channels. However, a major limitation of this smart systemic approach is its narrow line of investigation as far as the regime of the research area is concerned, i.e., alkali contents. More recently, Izzo et al. [16] have established a comprehensive information bank of 192 FTIR spectra of geomaterials for the mineralogical community. This data set offers a robust tool for gemstone identification and classification on the basis of properties like color and inclusion, morphism (Iso and poly), anisotropy (optical), crystallinity index, H_2O contents, and polyphysicity, etc. The associated functional groups were used for the estimation of all the abovementioned properties. However, still, more in-depth analysis is required to have a precise qualitative and quantitative analysis of gemstones from different localities.

In this paper, characterization of four natural gemstones including Quartz (colorless), Pyrope-Almandine Garnet (purplish-red), Black tourmaline, and Amethyst (light purple) brought from Hunza valley (Gilgit Baltistan) is performed. All four precious ornaments are primarily characterized with EDX spectroscopy for investigating the trace elements. Subsequent to EDX, FTIR spectroscopy was performed to identify the major functional groups in each sample. In addition, UV-VIS spectroscopy is performed to figure out the Urbach energy, direct and indirect bandgap energies of each stone. Actually, the main theme is to explore the electronic transitions responsible for the color origination and to develop the correlation among the electronic properties with the molecular ones. Furthermore, a Photoluminescence study was carried out to further investigate the trace elements and meaningful information about the identification of gemstones.

2. Experimental

2.1. Materials. Four natural gemstones which are investigated in this study are Quartz (colorless), Pyrope-Almandine Garnet (purplish-red), Black tourmaline, and Amethyst (light purple). These samples were brought from Hunza valley (Gilgit Baltistan), Pakistan. The information about the chemical composition of each stone is given below.

(i) Quartz is the most abundant mineral in the crust of Earth and is found in tetrahedron form, and its chemical composition is SiO2.

(ii) Pyrope-Almandine Garnet is a mixed variety of pyrope and almandine garnet, and its general formula is (Mg, Fe)3Al2(SiO4)3.

(iii) Tourmaline constitute the supergroup minerals and its general formula is $XY_3Z_6\,[T_6O_{18}][BO_3]_3V_3W$; In which X can be Na, K, Ca, Pb^{+2}; Y can be Li, Mg, Fe^{2+}, Mn^{2+}, Cu^{2+}, Al, V^{3+}, Cr^{3+}, Fe^{3+}, Mn^{3+}, Ti^{4+}; Z can be Mg, Fe^{2+}, Al, V^{3+}, Cr^{3+}, Fe^{3+}; T can be Si, B, Al; B =B; V can be OH, O; W can be OH, F^-, O^{2-}. Black tourmaline is a black color variety of tourmaline group, and its chemical formula is $NaFe_3[Al, Fe]_6[Si_6O_{18}][BO_3]_3[OH]_3OH$.

(iv) Amethyst is the purple color variety of Quartz and its composition is the same as that of Quartz. The purple color of Amethyst is caused by the traces of iron impurities or other transition elements.

All stones have been used as received without any further treatment.

2.2. Sample Characterization

2.2.1. EDX Testing. For the observation of trace elements within each stone, a small piece of each stone was crushed and examined under the scanning electron microscopy model JSM-5910 SEM (JEOL Company, Japan). The elemental composition of the samples was obtained through an EDS analysis by utilizing Field Emission Gun of Scanning Electron Microscope (FEG-SEM, SE-4300, Hitachi Co., Tokyo, Japan), which was equipped with an Electron Dispersive X-ray Diffraction (EDS) probe and a cathodoluminescent (CL). The accelerated voltage was 5 kV with magnification between 2,000X to 70,000X.

2.2.2. FTIR Testing. The infrared spectroscopy (in total attenuated reflectance mode) of pure all stones was performed in the laboratory by using Nicolet-6700 Fourier transform infrared spectrophotometer (Thermo Electron Corporation, Waltham, MA, USA) at a resolution of $4\,\mathrm{cm}^{-1}$ from $400\,\mathrm{cm}^{-1}$ to $6000\,\mathrm{cm}^{-1}$. The FTIR spectra were standardized and significant vibration groups were recognized and associated with the main chemical group. In order to reduce the signal-to-noise ratio (SNR), spectra were taken from three/four points and then averaged to have a single spectrum for each sample [17].

2.2.3. UV-VIS Testing. The stones under investigation were tested on Perkin Elmer DRS setup Model Lamda 950 equipped with a 150 mm integrating sphere, which is available at National Center for Physics, Islamabad, Pakistan. The reflectance measurements were carried out over the spectral range 250–100 nm and further processed to extract the spectroscopic and bandgap properties. The detail of processing the reflectance data is given below.

The absorption coefficients over the wavelength of interest are utilized for determining the Urbach energy and bandgap energies (Eg) [18]. The value of absorption coefficient at a particular wavelength is the ratio of absorption to sample thickness and is represented as α, i.e.,

$$\alpha = \frac{A}{d}, \tag{1}$$

where α is the absorption coefficient, A is the absorption, and d is the thickness of the sample.

For the calculation of Urbach energy which is denoted by Eu, the following relation is used [all relevant ref].

$$\alpha = \alpha_0 \exp^{(h\nu/E_u)}, \tag{2}$$

where α is the absorption coefficient, $h\nu$ is the photon energy.

The slope of the ln (a) vs. $h\nu$ plot in the lower photon energy region is used for the calculation of Eu of each sample. For the calculation of bandgap energies direct and/or indirect, modified Mott and Davis as reported in the literature [19, 20] is used.

$$\alpha h\nu = K\left(h\nu - E_g\right)^x, \tag{3}$$

where Eg is the bandgap energy and is either direct or indirect depending on the value of x, If $x = 1/2$, then the above equation gives the values of the allowed direct transition, If $x = 2$, then the above equation gives the value of indirect transitions, and K is a constant within the given frequency range.

For determination of direct and indirect transition, a graphical approach is used, where extrapolation of linear regions of $[\alpha h\nu]2$ and $[\alpha h\nu]1/2$ plots to Y axis = 0 on energy axis give the values of direct and indirect energy bands gaps. As α is proportional to the Kulekha–Munk function $F(R)$ given as follows:

$$[F(R)] = \frac{K}{S} = \frac{(1-R)^2}{2R}, \tag{4}$$

where $[F(R)]$ is remission or Kubelka-Munk function (KMF), R is reflectance, K is the absorption, S is the scattering from sample, respectively.

It is, therefore, used here for the calculation of Urbach energy and band gap properties.

2.2.4. Photoluminescence Testing. Photoluminescence is the process in which a substance absorbs electromagnetic radiation in the form of photons and reradiates photons. Quantum mechanically, it is defined as the excitation of electrons to higher energy states and then relaxes to lower energy states accompanied by emission of light. Photoluminescence spectroscopy measures the emission spectra, which reveals only the lower energy features. In this study, the gemstones were analyzed by Photoluminescence spectrometer DONGWOO OPTRONIC CO. Ltd. with a Laser exciting wavelength of 325 nm.

3. Results and Discussion

Chemical analysis of samples was carried out by SEM/EDX that revealed the concentration of each component element and impurity traces. The results of EDX are tabulated in Table 1 and it can be seen as follows:

(i) Traces of Ca, Mg and Fe in Pyrope-Almandine Garnet

(ii) Traces of Mg and Fe in Black tourmaline

(iii) Traces of Au and Ca in Amethyst

(iv) No trace elements or impurity contents were observed in Quartz.

In UV-VIS spectroscopy, the sample is irradiated by an ultraviolet and visible portion of the spectrum. When a certain band of UV-Visible spectrum matches the certain electronic transition of the sample, then it will be absorbed. The absorbed energy of the electron must be equal to the energy gap between the two levels; as a result of the aforementioned electronic transition phenomena, an absorption spectrum is obtained, called UV-VIS absorption spectrum. In the case of crystalline materials, the ultraviolet region of the spectrum reveals the interesting features of sample due the band to band transition. Among these

Table 1: Concentration of impurities within the gemstones characterized in this study.

Gem stone		Au	Ca	Mg	Fe	Na	Al	Si	O
Pyrope-almandine garnet	wt.%	—	1.09	3.63	20.00	—	10.57	17.15	47.56
	A%	—	0.60	3.31	7.94	—	8.59	13.54	65.92
Quartz	wt.%	—	—	—	—	—	—	48.10	60.90
	A%	—	—	—	—	—	—	26.78	73.22
Black tourmaline	wt.%	—	—	1.49	8.98	0.98	19.24	18.88	50.44
	A%	—	—	1.27	3.35	0.89	14.84	14.00	65.65
Amethyst	wt.%	4.68	0.66	—	—	—	—	53.31	41.34
	A%	0.53	0.37	—	—	—	—	41.97	57.14

Note. Boron was not detected in Black tourmaline EDX spectra due to low X-rays energy.

features, absorption edge close to short wavelength is of particular importance because this absorption is due to the excitation of electrons from the valence band to the conduction band [21, 22]. This transition from valance-to-conduction bands, i.e., absorption edge in the shorter wavelength region, has meticulous importance in the field of electronic structure. In addition to such absorption in the shorter wavelength or UV regions, the absorption in the visible region is responsible for the coloration of an object, and the color is the most attractive characteristic of gemstones that arise at different wavelengths. In most of the cases, transition metals (Fe, Mn, Co, Ni, Cu, Ti, Cr, V) are responsible for the coloration of gemstones due to the absorption of visible light. These transition metals can be present as part of impurities or as part of the chemical composition of gemstones. The transition metals have the partially filled d-orbital. When the wavelength having suitable energy raises the unpaired electron to higher energy states, the energy of such wavelength is completely absorbed by electrons, thus giving the absorption spectrum in gems due to d-orbital's transition. These transition metals are identified by the UV-VIS spectrum of gemstones in accordance with their specific absorption bands [23].

Figure 1(a) shows the UV-VIS spectrum of Pyrope-Almandine Garnet in which absorption peaks of Fe were observed in the visible region, Mg and Ca in UV region. Following are the identified absorption bands in the UV-VIS spectrum shown in Figure 1.

(i) The UV-VIS spectra of Pyrope-almandine garnet revealed the absorption bands of Ca at 266, 243, 228, and 205 nm, while Mg at 371, 336, 318, and 292 nm and Fe at 701, 574, 507, and 426 nm.

(ii) The Iron band at 701 nm is assigned to $^6A_{1g}$ (S) $\longrightarrow$ $^4T_{1g}$ (G) transition, the bands 574 nm and 507 nm are assigned to $^6A_{1g}$ (S) $\longrightarrow$ $^4T_{2g}$ (G) transitions, while the band 426 nm is assigned to $^6A_{1g}$ (S) $\longrightarrow$ $^4A_{1g}$ (G), ^4E_g (G) transition.

The EDX data shown in Table 1 and documented results in the literature [24, 25] are in agreement with our findings. Furthermore, the higher concentration of Fe, i.e., 20% by weight within the matrix of this gem stone, is the reason for the purplish-red color of Pyrope-Almandine Garnet (see Figure 2). Shown in Figure 1(b) is the UV-VIS spectrum of Quartz. It shows only one absorbance peak at 321.9 nm, which belongs to SiO2 absorbance, thus complementing the EDX results given in Table 1. From Figure 1(c), it was observed that the UV-visible spectra of Black tourmaline revealed the absorption bands of Mg at wavelengths of 263, 301, 340, 351, and 381 nm and Fe at 437, 469, 532, and 701 nm. The iron band 701 nm is assigned to $^6A_{1g}$ (S) $\longrightarrow$ $^4T_{1g}$ (G) transition, the band 532 nm is assigned to $^6A_{1g}$ (S) $\longrightarrow$ $^4T_{2g}$ (G) transition, while the bands 469 nm and 437 nm are assigned to $^6A_{1g}$ (S) $\longrightarrow$ $^4A_{1g}$ (G), ^4E_g (G) transitions, respectively. The spectrum of Amethyst is shown in Figure 1(d), which revealed the absorption band of Au at 550 nm, which is assigned to ^2E_g (2D) $\longrightarrow$ $^2T_{2g}$ (2D) transition and the Ca bands revealed at 344, 309, and 272 and 256 nm. As impurities of iron changes the purple color to Amethyst, but Amethyst used in this study has a light purple color and revealed the weak absorption of Au impurities at 550 nm. Therefore, it means that very weak absorption of Au in the visible region may cause the light purple color in Amethyst, and thus, in this case, Au impurities cause the light purple color in Amethyst. The results of EDX shown in Table 1 are in total agreement with the UV-VIS spectroscopy.

Urbach energies (Eu) or the optical activation energies of the gemstone, which are calculated from UV-VIS absorption spectra, are given in Table 2. Urbach energy was calculated from the plot of $\ln[F(r)]$ (shown in Figure 3) on the y axis versus the photon energy on the x-axis while calculating the reciprocal of the slopes of the linear portion in the shorter wavelength region. The reason for choosing the Kublekha Munk function for the calculation of Urbach energy is the linear dependence of $F(R)$ on the absorption coefficient α. Urbach energy is among the important parameters as far as optical transitions are concerned and has a correlation to the structural disorder of the material under investigation. This means that the higher value of Urbach energy reveals a low crystalline structure while a smaller value reveals a higher crystalline structure. Thus, Urbach energy indicates the structural disorder or imperfection in materials. These structural imperfections arise due to the formation of localized energy states close to the boundaries of the energy gap. Urbach energy is also inversely proportional to the optical band gap energy [18, 19]. The values of Urbach energies of Pyrope-Almandine garnet, Quartz, Black tourmaline, and Amethyst are 0.52 eV, 0.21 eV, 0.46 eV, and 0.43 eV, respectively. The smaller value of Urbach energy for

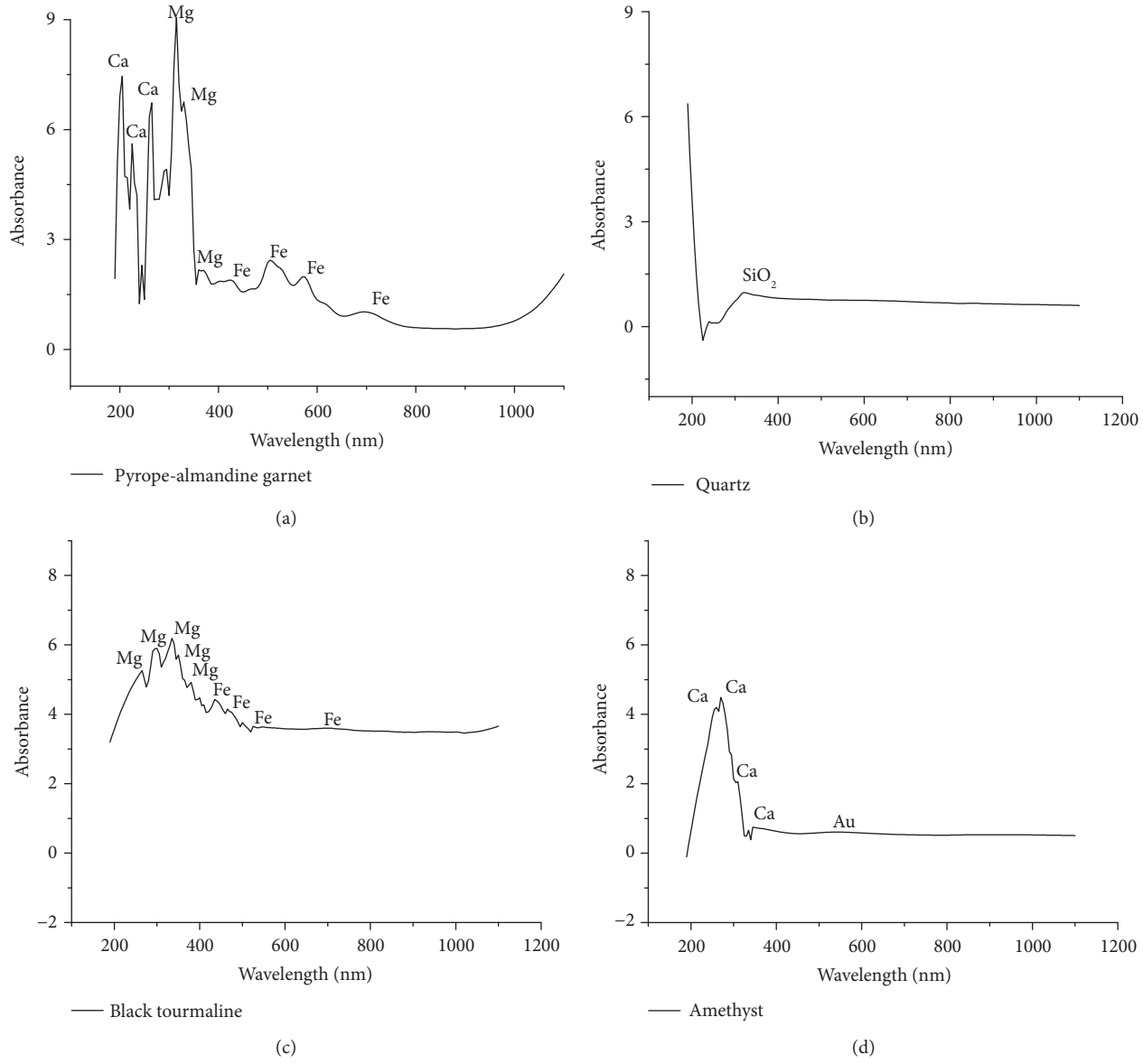

Figure 1: UV-VIS spectrum of (a) pyrope-almandine garnet, (b) Quartz, (c) Black tourmaline, and (d) Amethyst.

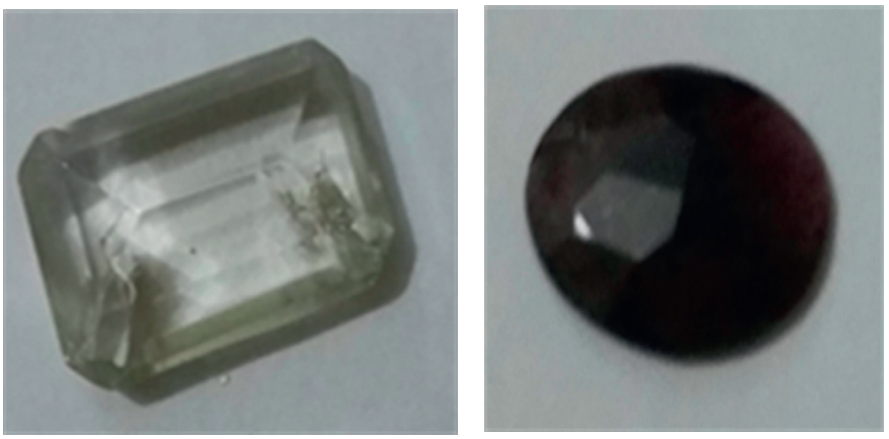

Figure 2: Continued.

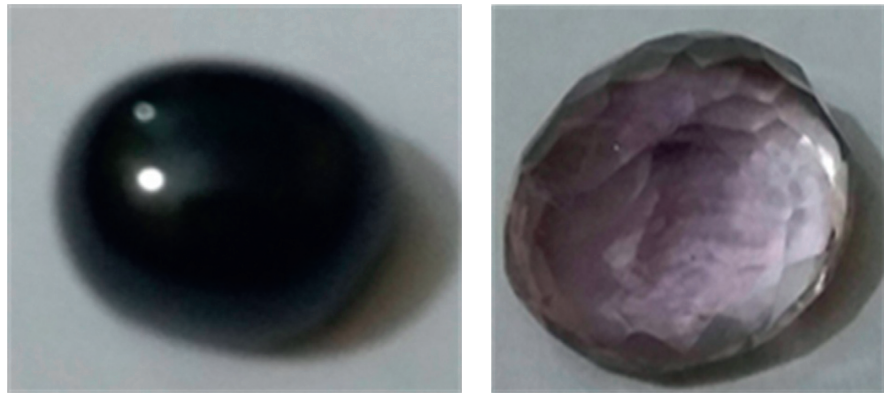

(c) (d)

Figure 2: Screen shots of stone investigated in this study: (a) Quartz (10 Ct) (b) Pyrope-almandine garnet (5Ct), (c) Black tourmaline (30 Ct), and (d) Amethyst (5 Ct).

Table 2: Urbach energy of gemstones calculated by the slope of the best fit line through vertical segments of plots from Figure 3

Samples	Slope	Urbach energy (meV)
Pyrope-almandine garnet	1.93	520
Quartz	4.75	210
Black tourmaline	2.17	460
Amethyst	2.32	430

Table 3: Direct bandgap energy is calculated by extra plotting the vertical segment of the plot with intercept x-axes from Figure 4.

Sample	Direct band gap energy (eV)
Pyrope-amandine garnet	5.14
Quarts	6.12
Black tourmaline	5.54
Amethyst	5.74

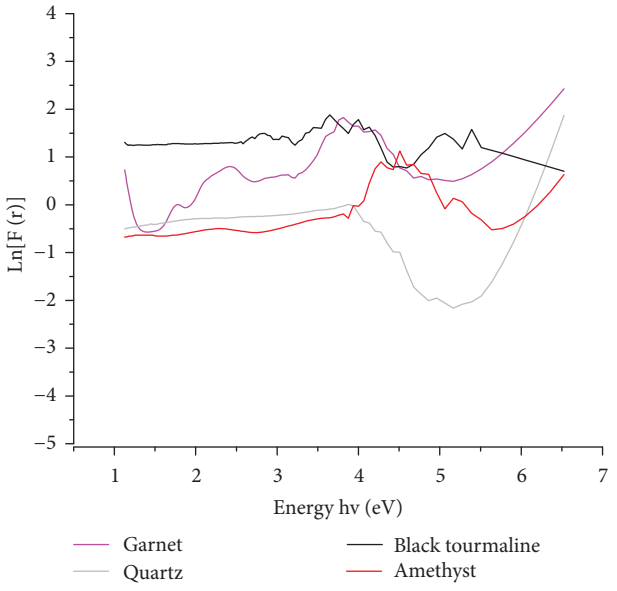

Figure 3: Plot of ln[$F(r)$] versus Photon energy (hν) for the calculation of Urbach energy.

Quartz, i.e., 0.21 eV reveals the fact that Quartz sample used in this study has the high crystalline structure with almost negligible traces of impurities. Further, the observation is consistent with the recently reported Urbach energy range of SiOx for $x < 2$, i.e., 0.172–0.523 eV depending upon the contents of oxygen [26]. Pyrope-Almandine Garnet has a higher value of Urbach energy which shows a low crystalline structure compared to Quartz and is also evidence of higher impurity contents. The EDX data of Pyrope-Almandine Garnet also agree with our finding of higher values of Urbach energy and structural disorder. The value of Urbach energy of Pyrope-Almandine Garnet found in this study is 520 meV. That is, it might be due to the higher percentage of Fe by weight, i.e., ~ 20% by weight (see Table 1). The reported results of Urbach energy for Fe oxide by Zhao et al. [27] are in good agreement with our finding for this gemstone. The values of Urbach energy for Black tourmaline and Amethyst are 0.46 and 0.43 eV, respectively. These values are also higher and evident by the presence of impurities within these samples. The value of Urbach energy for Black tourmaline might belong to the Mg contents present in this sample as it is recently reported by Singh et al. [28] that the sample containing the 50% contents of Mg+2 has the value of Urbach energy to 0.46 eV. The values of Urbach energy for Amethyst might be due to the Ca.

Direct bandgap energies of all gemstones were calculated by plotting the $[F(r)xh\nu]2$ as a function of photon energy hν. Afterward, extra plotting the vertical segments of the plot to intercept the x-axes gave the bandgap energies shown in Figure 5. As the absorption coefficient is directly proportional to the absorbance $F(r)$; therefore, here in this study, F(R) is used for calculating the energy band gaps. The calculated values of bandgap energies of all gemstones are given in Table 3. Pyrope-Almandine Garnet showed a bandgap energy of 5.14 eV, which is attributed to SiO2 that is the major component of garnet. The decrease in bandgap energy is due to the presence of impurities of Fe, Mg, and Ca, as found from EDX data. The value of bandgaps for Quartz

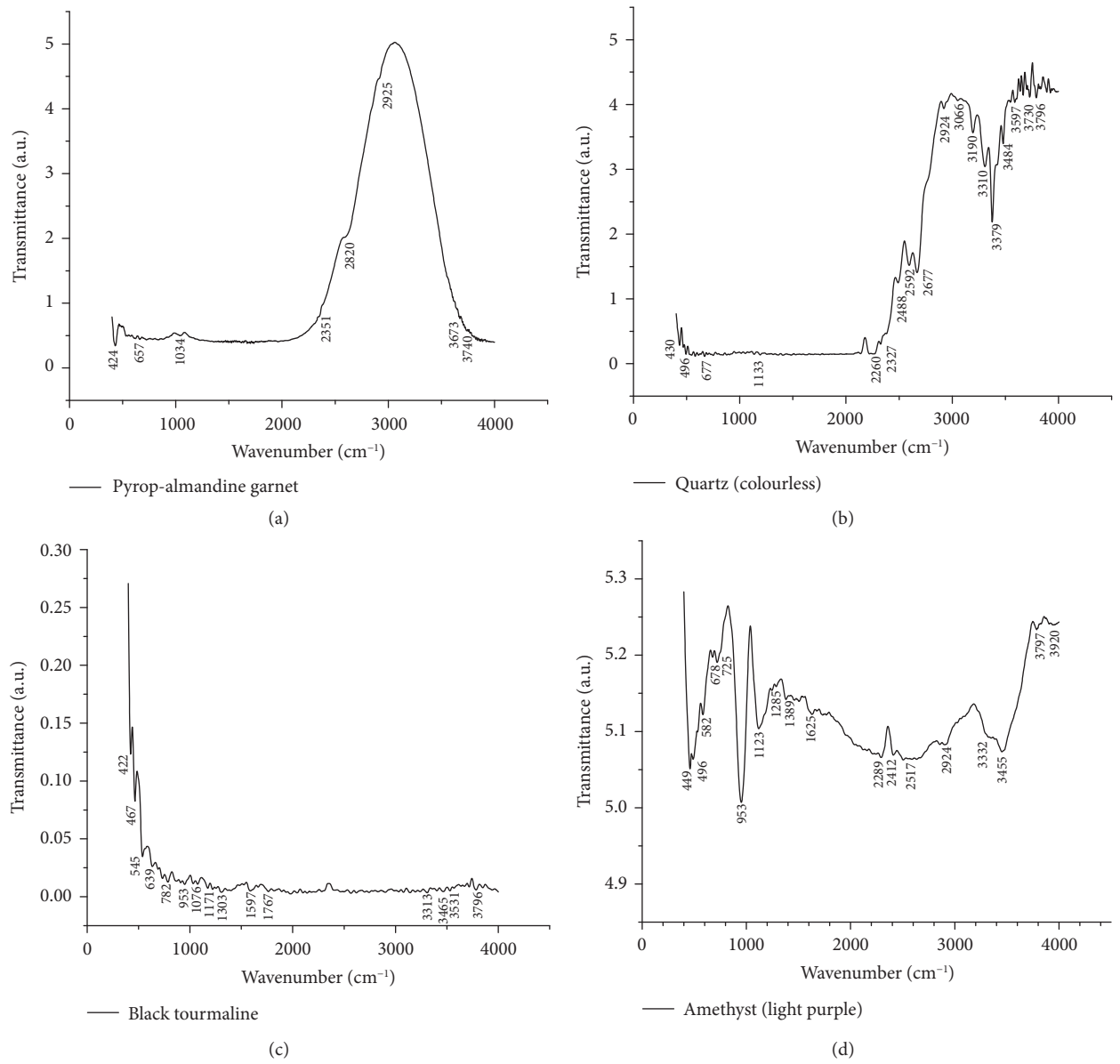

Figure 4: FTIR spectra of (a) pyrope-almandine garnet, (b) Quartz, (c) Black tourmaline, and (d) Amethyst.

found in this study is 6.12 eV (see Table 3), which in total agreement with the values reported in the literature, i.e., 6.3 eV [29, 30]. Black tourmaline revealed the bandgap energy of 5.54 eV. As SiO2 is the major component of Black tourmaline; therefore this bandgap 5.54 eV is attributed to SiO2. Amethyst revealed a bandgap energy of 5.74 eV. Amethyst is the purple color variety of Quartz due to the presence of Fe impurities. In this study, Amethyst revealed the impurities of Au and Ca that caused the decrease in the bandgap energy of Amethyst. The inverse proportion of Urbach energy with the direct band gaps energies is also in agreement with the literature [29].

FTIR spectra of all gemstones under investigation are shown in Figure 4. Pyrope-Almandine Garnet revealed FTIR-vibrational bands at 424, 657, 1034, 2351, 2630, and 2925 cm^{-1}. In addition to these bands, very small absorption bands at 3673 and 3740 cm^{-1} are also there in the FTIR spectra of Pyrope-Almandine Garnet (see Figure 4). Vibrational peaks observed at 424 cm^{-1} and 657 cm^{-1} are attributed to Fe-O. The peak at 1034 cm^{-1} occurred due to Si-O stretching vibration. The stretching vibration of C=O observed at 2334 cm^{-1}, while peaks at 2820 and 2925 cm^{-1} may be resulted due to O-H stretching vibrations or might be caused by other impurities [25]. The smaller peaks observed at 3673 and 3740 cm^{-1} might be due to Fe-OH-vibrations [31].

Figure 4 shows the FTIR spectra of Quartz, in which absorption peaks at 430, 496, and 677 cm^{-1} are attributed to Si-O bending vibrations, while the peak at 1113 cm^{-1} is attributed to stretching vibration of Si-O [32, 33]. The bands that appeared at 2260 and 2327 cm^{-1} are attributed to weak Si-OH-vibrations [34]. Strong bands at 2488, 2592,

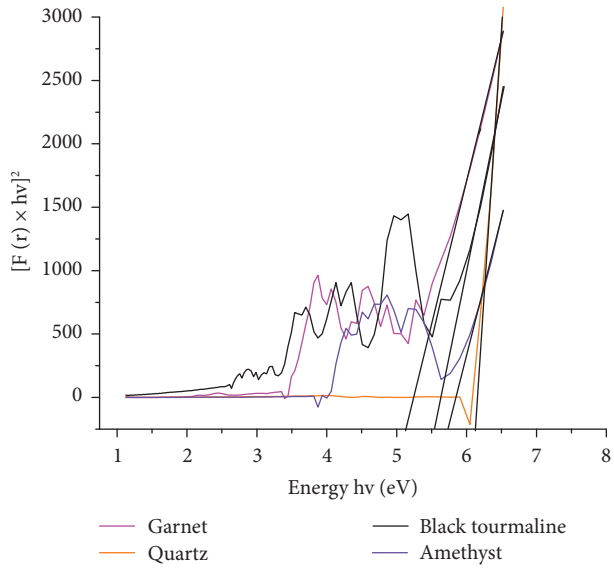

FIGURE 5: Plot of $[F(r)xh\nu]2$ versus photon energy shows the direct bandgap energies of the garnet, Quartz, Black tourmaline, and Amethyst.

and 2677 cm^{-1} are observed due to Si-O stretching. In addition to this, strong bands were observed at 2924 and 3066 cm^{-1}, which are always present in Quartz according to previous literature [35]. The origin of these bands might be the O-H stretching vibration. The bands observed at 3190 and 3310 are attributed to Si-O stretching, the bands at 3379 cm^{-1} and 3381 cm^{-1} are ascribed to Al-OH and AlSi-OH/Li-vibrations, respectively [36], since Al3+ and Fe3+ replace the Si4+ in the center of SiO4 tetrahedron and designated as AlSi3+ or FeSi3+, the charge deficiency is fulfilled by interstitial monovalent ions (H+, Li+ and Na+) considered as charge compensators. The band at 3597 cm^{-1} is ascribed to AL-OH/Na stretching vibration [37]. Typical noise was observed between regions of 3600 and 4000 cm^{-1} in accordance with previous literature [38]. It is also possible that the bands appeared at 3730 and 3796 cm^{-1} and in this region may be resulted due to the presence of Fe-OH-vibration.

Figure 4(c) shows the spectra of Black tourmaline, in which the main bands observed at 422, 467, 545, and 639 cm^{-1} are attributed to Si-O-Si bending vibrations, B-O bending vibration, and M-O stretching vibrations (where M can be Fe or Al). The band at782 cm^{-1} is attributed to Si-O-Si stretching vibration; the bands observed at 953, 1076, and 1171 cm^{-1} are attributed to Si-O stretching vibrations. The bands appearing at 1303 and 1397 cm^{-1} are attributed to B-O stretching vibrations. The bands at 1597 and 1767 cm^{-1} might be due to C=O stretching vibrations, while the band at 3313 cm^{-1} is ascribed to O-H stretching vibration. The bands at 3465 and 3531 cm^{-1} are attributed to the stretching vibrations of M-OH3 bonds in ^{y}Fe ^{z}Al ^{z}Al environment (where M represents Fe and Al). The band at 3796 cm^{-1} is ascribed to strong stretching vibration of M-OH bond in ^{y}Fe ^{y}Fe ^{y}Fe environment (where M represent Fe). All these vibrations of Black tourmaline are in good agreement with previous literature [39].

Figure 4(d) shows the spectra of Amethyst. As Amethyst is a purple color variety of Quartz due to the presence of iron impurities, therefore, some of its FTIR bands can be correlated with Quartz and the bands may vary within 10–20 cm^{-1}. The less intense bands at 449, 496, 582, 678, and 725 cm^{-1} are attributed to Si-O bending and some bands might be due to Ca-O stretching vibrations, while the intense bands at 953 and 1123 cm^{-1} attributed to Si-O strong stretching vibrations, the bands at 1285 and 1389 cm^{-1} are attributed to Si-OH weak-vibrations, the band at 1625 cm^{-1} might be resulted due to C=O stretching vibration, the bands appeared at 2289 cm^{-1} attributed to Si-OH weak-vibration, bands at 2412, 2517 and 2924 cm^{-1} are attributed to Si-O stretching vibrations. The band at 3332 cm^{-1} is attributed to Al_{Si}-OH-vibration, the band at 3455 cm^{-1} attributed to Al_{Si}-OH/Na-vibration, the bands at 3579.1 to 3580.5 cm^{-1}, 3395.2 to 3415.4 $cm^{-1,}$ and 3351.5 to 3354.4 cm^{-1} are probably related to iron according to previous literature [37], but these bands are not observed in Amethyst sample. The bands at 3787 and 3920 cm^{-1} may be attributed to Fe-OH stretching vibrations.

Absorption spectra measure the absorbed energy of electrons when they jump from lower energy states to higher energy states, while emission spectra measure the releasing energy of electrons when they jump from higher energy states to lower energy states as the absorption spectrum encounters the excitation energy when electrons jump from ground state S_0 to higher energy states $S_{1,}$ $S_{2,}$ $S_{3,}$ $S_{4,}$ etc. Thus, it reveals the absorption of higher energy states and lower energy states and exposes detailed information about the optical properties and impurities content of a sample. On the other hand, PL spectroscopy takes a case of emitted light that comes due to the transition of lowest energy state S_1 to ground state $S_{0.}$ When an atom or molecule is excited to higher energy states, it ends up in the lowest energy state S_1 while emitting radiations, then the emission and absorption

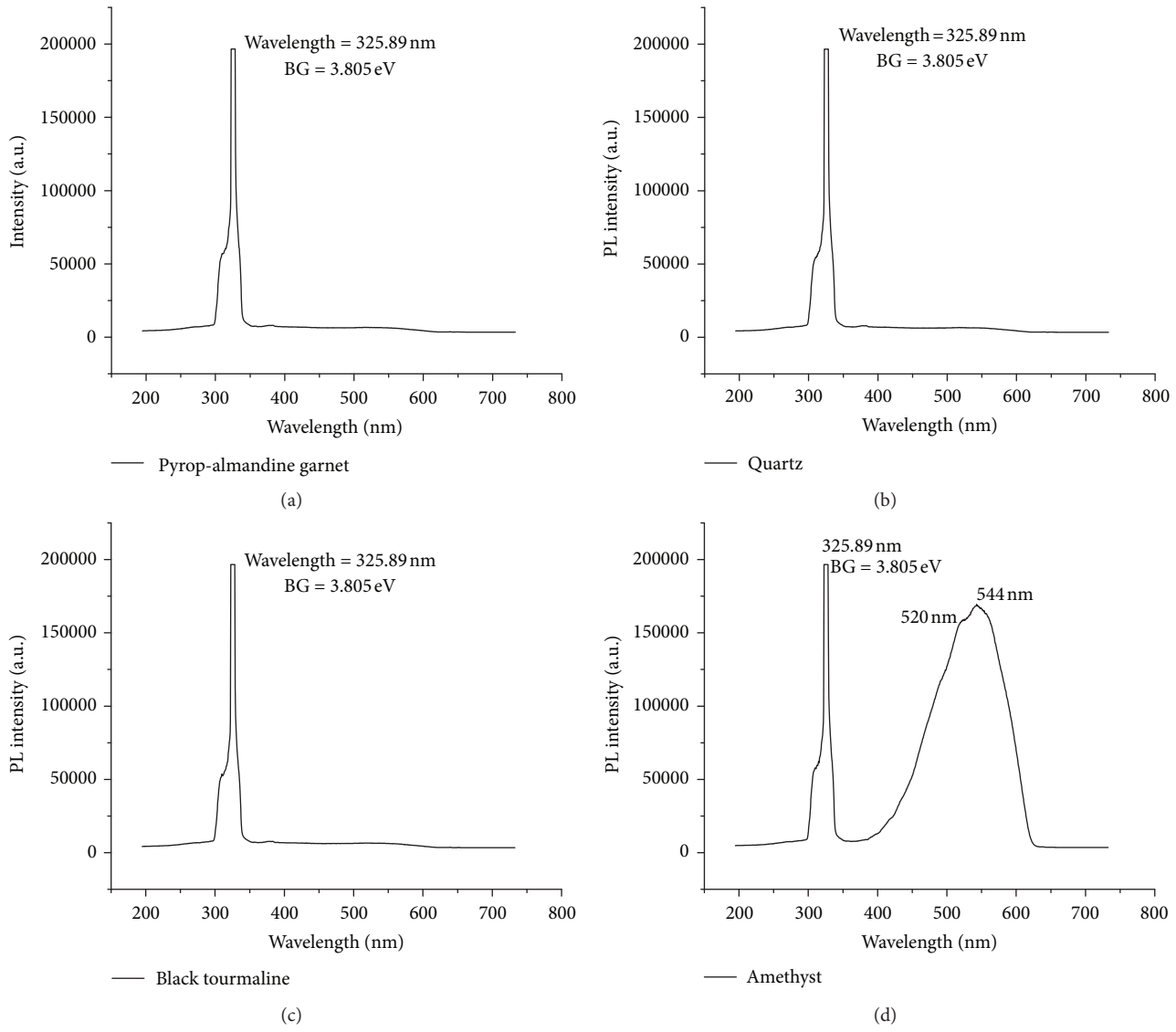

Figure 6: Photoluminescence (PL) spectra of (a) pyrope-almandine garnet, (b) Quartz, (c) Black tourmaline, and (d) Amethyst.

spectrum will be the same. However, if an atom directly goes to the ground state without ends up in the lowest energy state then it only reveals the lowest energy features. The absorption spectrum shows the S_0–S_1, S_0–S_2, S_0–S_3 bands while the emission spectrum shows only S_0- S_1 band [40, 41]. Mostly the colors of gemstones are caused by the transition elements due to the absorption of visible light, and these transition metals can be present as impurities or as compositional parts of gemstones. Therefore, our UV-Visible absorption spectra of all four gemstones: pyrope-almandine garnet, Quartz, Black tourmaline, and Amethyst have shown the absorption bands of Ca, Mg, Fe, and Au both as impurities and compositional constituents (see Figures 1(a)–1(d)). However, for PL spectra, the situation is different as it only encounters the emitted light due to the transition of electrons from lowest energy states S_1 to the ground state S_o. The bands of Ca, Mg, and Fe in pyrope-almandine garnet, Mg and Fe in Black tourmaline, and Ca in Amethyst are not present in PL spectra in spite of the fact that all of the above are found as compositional elements from UV-Vis spectra shown in Figure 1, e.g., Fe and Mg in pyrope-almandine garnet, Ca and Fe in Black tourmaline, while Mg and Ca in Amethyst. A PL spectra only encounter the emission light due to the relaxation of electrons from lowest energy state S_1 to ground state S_o and reveal the lower energy features, and also the direct transition from higher energy states to ground state cannot be measured by PL spectroscopy. In addition to this, some molecules absorb the radiations but do not emit light. It is, therefore, the bands of Ca, Mg, and Fe in pyrope-almandine garnet, Mg and Fe in Black tourmaline, and Ca in Amethyst are not there in PL spectra. However, emission bands of Au at the wavelength of 522 and 544 nm are there in PL spectra of Amethyst as an impurity due to the low energy feature of Au (see Figures 6(a)–6(d)). The bandgap energy is calculated by converting the emission onset wavelength from the lower wavelength side into electron volts. It is worth mentioning here that bandgap energy obtained by PL spectra is always less than the original band gap as it

measures only the lowest energy transition from S_1 to S_o. Therefore, it only reveals lower energy features. In Photoluminescence spectra of all four gemstones: pyrope-almandine, Quartz, Black tourmaline, and Amethyst, the main emission bands are observed at the same wavelength 325.89 nm that slightly shifted toward a longer wavelength compared to absorption bands shown in Figures 1(a)–1(d). The main emission band at 325.89 nm is also responsible for the bandgap of the gemstones and attributed to the SiO_2 as all the samples contain SiO_2 as a major component. Conversion of wavelength 325.89 nm into energy by $E = hc/\lambda$ gave the bandgap energy of 3.805 eV for each sample. All the gemstones revealed the same bandgap energy due to SiO_2 as the dominant constituent. The most important observation here is that emission bandgap energy is less than the absorption bandgap energy which is due to the energy differences between the absorbed and emitted radiations. In this case, both the emission and absorption spectra differ from each other due to different transitions. The emission spectra and absorption spectra can be the same only if a molecule is excited to higher energy states and it often ends up in the lowest energy state S_1 and then returns to the ground state with the emission of light.

Photoluminescence emission peaks of gold are observed in the range of 400–653 nm depending on the interfering medium (ligand) and exciting wavelength. Ligand induces little changes in the electronic structure of the gold, which causes the ligand to metal charge transfer transition due to which emission fundamentally arises from molecular gold and few from the atoms. There are two major accepted explanations about the Photoluminescence mechanism:

(i) One is the pure metal quantum confinement effect Photoluminescence emission of pure metal originated from sp-sp and sp-d transitions.

(ii) The other explanation is the charge transfer due to the interaction between functional ligand and metal, i.e., the ligand to metal charge transfer (LMCT) and ligand to metal-metal charge transfer (LMMCT).

Luminescence dominantly is ascribed to the LMCT effect rather than the LMMCT effect. However, increasing the electro positivity of metal can promote the interaction between ligand and metal. Photoluminescence emission peaks position can be altered due to ligand to metal charge transfer transition (LMCT) or metal to ligand charge transfer (MLCT). The charge can be transferred from ligand to metal if the ligand has field orbital and metal has the vacant orbital, while in other cases, the charge can be transferred from metal to ligand if the ligand has the vacant orbital and metal has the field orbital. Here, in this study, for the case of Amethyst, Photoluminescence spectra emission peaks of gold were observed at 522 and 544 nm because SiO_2 is the ligand for this case, which contains the electron-rich oxygen atom. It is, therefore, the emissions peaks of gold at 522 and 544 nm might be assigned to the ligand to metal charge transfer transition, i.e., electron transfer from oxygen to gold [42–44].

4. Conclusion

SEM/EDX was used to evaluate the chemical composition and hence the trace elements of all gems. SEM/EDX results revealed traces of Fe, Mg, and Ca in Pyrope-Almandine garnet, Mg and Fe in Black tourmaline, Au and Ca in Amethyst, whereas no impurities were detected in Quartz. The UV-Visible technique was successfully employed to identify the trace elements of all samples through their absorption spectra with their corresponding absorption peaks, and to confirm the decency of EDX data of particular importance, data on the Urbach and bandgap energies were reported for the first time, to the best of our knowledge, to explore the effects of impurities/trace elements on the structural and electronic structure of these gemstones. Furthermore, FTIR spectroscopy is also successfully used to characterize the gems to identify the functional group and molecular vibrations by their respective band position with more reliable values. Photoluminescence results were successfully interpreted in correlation with UV-Visible spectroscopy, and it also showed meaningful information about the identification of gemstones.

Data Availability

The data will be made available upon request to the corresponding author.

Conflicts of Interest

The authors declare that they have no conflicts of interest.

Acknowledgments

Dr. Malik Sajjad Mehmood would like to acknowledge the University of Engineering and Technology, Taxila and Pakistan Institute of Engineering and Applied Sciences, Islamabad, Pakistan, for providing the platform to complete this research work.

References

[1] C. M. Breeding, A. H. Shen, S. Eaton-Magaña, G. R. Rossman, J. E. Shigley, and A. Gilbertson, "Developments in gemstone analysis techniques and instrumentation during the 2000s," *Gems & Gemology*, vol. 46, no. 3, pp. 241–257, 2010.

[2] S. De Meo, A. Plutino, and A. Rizzi, "Assessing color of gemstones," *Color Research & Application*, vol. 45, no. 2, pp. 224–234, 2020.

[3] B. Devouard and F. Notari, "The identification of faceted gemstones: from the naked eye to laboratory techniques," *Elements*, vol. 5, no. 3, pp. 163–168, 2009.

[4] E. Fritsch and B. Rondeau, "Gemology: the developing science of gems," *Elements*, vol. 5, no. 3, pp. 147–152, 2009.

[5] E. Fritsch and G. R. Rossman, "An update on color in gems. part 1: introduction and colors caused by dispersed metal ions," *Gems & Gemology*, vol. 23, no. 3, pp. 126–139, 1987.

[6] E. Fritsch and G. R. Rossman, "An update on color in gems. part 3: colors caused by band gaps and physical phenomena," *Gems & Gemology*, vol. 24, no. 2, pp. 81–102, 1988.

[7] R. J. Tilley, *Colour and the Optical Properties of Materials*, John Wiley & Sons, Hoboken, NJ, USA, 2020.

[8] T. W. Overton and J. E. Shigley, "A history of diamond treatments," in *The Global Diamond Industry*, pp. 181–228, Springer, Berlin, Germany, 2008.

[9] S. Karampelas, B. Al-Shaybani, F. Mohamed, S. Sangsawong, and A. Al-Alawi, "Emeralds from the most important occurrences: chemical and spectroscopic data," *Minerals*, vol. 9, no. 9, p. 561, 2019.

[10] D. Skoog, F. J. Holler, and S. Crouch, *Principles of Instrumental Analysis*, Thomson Brooks Cole, San Francisco, CA, USA, 2007.

[11] S. Karampelas, E. Fritsch, J.-P. Gauthier, and T. Hainschwang, "UV-Vis-NIR reflectance spectroscopy of natural-color salt-water cultured pearls from Pinctada margaritifera," *Gems & Gemology*, vol. 47, no. 1, pp. 31–35, 2011.

[12] P. Mazzoleni, G. Barone, S. Raneri, E. Aquilia, D. Bersani, and R. Cirrincione, "Application of micro-Raman spectroscopy for the identification of unclassified minerals preserved in old museum collections," *Pliniu*, vol. 42, pp. 112–124, 2016.

[13] K. Chang, S. Lee, J. Park, and H. Chung, "Feasibility for non-destructive discrimination of natural and beryllium-diffused sapphires using Raman spectroscopy," *Talanta*, vol. 149, pp. 335–340, 2016.

[14] S. M. Kassem, A. Rashad, G. Ahmed, R. A. Fahim, S. Salem, and S. Ebraheem, "Spectroscopic analysis of irradiated natural quartz and ESR dating aspects," *Arab Journal of Nuclear Sciences and Applications*, vol. 53, no. 3, p. 197, 2020.

[15] C. Branca, A. Arcovito, E. Cosio et al., "Combining Fourier transform infrared and Raman spectroscopies with Gaussian deconvolution: an improved approach for the characterization of emeralds," *Journal of Raman Spectroscopy*, vol. 51, no. 4, pp. 693–701, 2020.

[16] F. Izzo, C. Germinario, C. Grifa, A. Langella, and M. Mercurio, "External reflectance FTIR dataset (4000-400 cm^{-1}) for the identification of relevant mineralogical phases forming Cultural Heritage materials," *Infrared Physics & Technology*, vol. 2020, Article ID 103266, 2020.

[17] M. S. Mehmood, A. Sanawar, N. Siddiqui, and T. Yasin, "Quantification of silane grafting efficacy, weak IR vibration bands and percentage crystallinity in post e-beam irradiated UHMWPE," *Polymer Bulletin*, vol. 74, no. 1, pp. 213–227, 2017.

[18] M. S. Mehmood, I. Thira, A. Idris, T. Yasin, and M. Ikram, "UHMWPE bandgap properties -II: effect of post e-beam irradiation real time shelf aging in air," *Radiation Physics and Chemistry*, vol. 159, pp. 231–237, 2019.

[19] M. S. Mehmood, N. Siddiqui, S. A. Maqbool, M. A. Baluch, S. S. Mukhtar, and T. Yasin, "Assessment of γ-sterilization and/or cross linking effects on orthopedic biomaterial using optical diffuse reflectance spectroscopy," *Optik*, vol. 144, pp. 387–392, 2017.

[20] N. F. Mott and E. A. Davis, *Electronic Processes in Non-crystalline Materials*, Oxford University Press, Oxford, UK, 2012.

[21] Y. Xu and M. A. A. Schoonen, "The absolute energy positions of conduction and valence bands of selected semiconducting minerals," *American Mineralogist*, vol. 85, no. 3-4, pp. 543–556, 2000.

[22] J. Jasieniak, M. Califano, and S. E. Watkins, "Size-dependent valence and conduction band-edge energies of semiconductor nanocrystals," *ACS Nano*, vol. 5, no. 7, pp. 5888–5902, 2011.

[23] D. Fisher, S. J. Sibley, and C. J. Kelly, "Brown colour in natural diamond and interaction between the brown related and other colour-inducing defects," *Journal of Physics: Condensed Matter*, vol. 21, no. 36, Article ID 364213, 2009.

[24] N. Sultana and S. P. Podila, "Almandine gemstone-a review," 2018.

[25] S. Sangsawong, V. Raynaud, and V. Pardieu, *Purple Pyrope-Almandine Garnet from Mozambique*, Gemological Inst Amer 5345 Armada Dr, Carlsbad, CA 92008, USA, 2016.

[26] J. O. Carneiro, F. Machado, L. Rebouta et al., "Compositional, optical and electrical characteristics of SiOx thin films deposited by reactive pulsed DC magnetron sputtering," *Coatings*, vol. 9, no. 8, p. 468, 2019.

[27] Y. Zhao, M. E. Sadat, A. Dunn et al., "Photothermal effect on Fe3O4 nanoparticles irradiated by white-light for energy-efficient window applications," *Solar Energy Materials and Solar Cells*, vol. 161, pp. 247–254, 2017.

[28] J. Singh, V. Verma, R. Kumar, and R. Kumar, "Influence of Mg2+-substitution on the optical band gap energy of Cr2–xMgxO3 nanoparticles," *Results in Physics*, vol. 13, Article ID 102106, 2019.

[29] E. Güler, G. Uğur, Ş. Uğur, and M. Güler, "A theoretical study for the band gap energies of the most common silica polymorphs," *Chinese Journal of Physics*, vol. 65, no. 1, 2020.

[30] E. Calabrese and W. B. Fowler, "Electronic energy-band structure of α quartz," *Physical Review B*, vol. 18, no. 6, pp. 2888–2896, 1978.

[31] T. Gonzalez-Carreño, M. Fernandez, and J. Sanz, "Infrared and electron microprobe analysis of tourmalines," *Physics and Chemistry of Minerals*, vol. 15, pp. 452–460, 1988.

[32] J. Hlavay, K. Jonas, S. Elek, and J. Inczedy, "Characterization of the particle size and the crystallinity of certain minerals by IR spectrophotometry and other instrumental methods-II. investigations on quartz and feldspar," *Clays and Clay Minerals*, vol. 26, no. 2, pp. 139–143, 1978.

[33] T. H. Ko and H. Chu, "Spectroscopic study on sorption of hydrogen sulfide by means of red soil," *Spectrochimica Acta Part A: Molecular and Biomolecular Spectroscopy*, vol. 61, no. 9, pp. 2253–2259, 2005.

[34] U. Henn and R. Schultz-Güttler, "Review of some current coloured quartz varieties," *The Journal of Gemmology*, vol. 33, no. 1, pp. 29–43, 2012.

[35] F. S. Lameiras, "The relation of FTIR signature of natural colorless quartz to color development after irradiation and heating," *Infrared Radiation*, pp. 41–56, InTech, Rijeka, Croatia, 2012.

[36] E. H. M. Nunes, F. S. Lameiras, M. Houmard, and W. L. Vasconcelos, "Spectroscopic study of natural quartz samples," *Radiation Physics and Chemistry*, vol. 90, pp. 79–86, 2013.

[37] F. S. Lameiras, E. H. M. Nunes, and W. L. Vasconcelos, "Infrared and chemical characterization of natural amethysts and prasiolites colored by irradiation," *Materials Research*, vol. 12, no. 3, pp. 315–320, 2009.

[38] E. H. Nunes, V. Melo, F. Lameiras et al., "Determination of the potential for extrinsic color development in natural colorless quartz," *American Mineralogist*, vol. 94, no. 7, pp. 935–941, 2009.

[39] M. Mercurio, M. Rossi, F. Izzo et al., "The characterization of natural gemstones using non-invasive FT-IR spectroscopy: new data on tourmalines," *Talanta*, vol. 178, pp. 147–159, 2018.

[40] R. Paschott, *"Photoluminescenc" in the Encyclopedia of Physics and Technology*, Vol. 1, Wiley VCH, Weinheim, Germany, 2008.

[41] X. L. Wu, G. G. Siu, C. L. Fu, and H. C. Ong, "Photoluminescence and cathodoluminescence studies of stoichiometric and oxygen-deficient ZnO films," *Applied Physics Letters*, vol. 78, no. 16, pp. 2285–2287, 2001.

[42] T.-Q. Yang, B. Peng, B.-Q. Shan et al., "Origin of the photoluminescence of metal nanoclusters: from metal-centered emission to ligand-centered emission," *Nanomaterials*, vol. 10, no. 2, p. 261, 2020.

[43] M. Pattabi and R. M. Pattabi, "Photoluminescence from gold and silver nanoparticles," *Nano Hybrids*, vol. 6, pp. 1–35, 2014.

[44] J. Liu, P. N. Duchesne, M. Yu et al., "Luminescent gold nanoparticles with size-independent emission," *Angewandte Chemie International Edition*, vol. 55, pp. 1–6, 2016.